Preparation and characterization of *Nephila clavipes* tubuliform silk gut

Víctor Ruiz[a,b,#], Ping Jiang[c,#], Claudia Müller[a,b], Inmaculada Jorge[d,e], Jesús Vázquez[d,e], Álvaro Ridruejo[b], Salvador D. Aznar-Cervantes[f], José Luis Cenis[f], Luis Messeguer-Olmo[g], Manuel Elices[b], Gustavo Víctor Guinea[a,b,h], José Pérez-Rigueiro[a,b,h,*]

a. Centro de Tecnología Biomédica. Universidad Politécnica de Madrid. 28223 Pozuelo de Alarcón (Madrid). Spain

b. Departamento de Ciencia de Materiales. ETSI Caminos, Canales y Puertos. Universidad Politécnica de Madrid. 28040. Madrid. Spain

c. College of Life Sciences. Jiangangshan University. Jiangxi Province. Ji'an. 343009. China.

d. Cardiovascular Proteomics Laboratory, Centro Nacional de Investigaciones Cardiovascular (CNIC), 28029, Madrid, Spain

e. Centro de Investigación Biomédica en Red de Enfermedades Cardiovasculares (CIBER-CV). 28029, Madrid. Spain.

f. Departamento de Biotecnología. Instituto Murciano de Investigación y Desarrollo Agrario y Alimentario (IMIDA), 30150, La Alberca, Murcia, Spain

g. UCAM-Universidad Católica San Antonio de Murcia. Regeneration and Tissue Repair Group. 30107, Guadalupe (Murcia), Spain.

h. Biomedical Research Networking Center in Bioengineering, Biomaterials and Nanomedicine (CIBER-BBN). Madrid. Spain.

# Both authors contributed equally to this work

* Corresponding author

Keywords: Biomimetics; mechanical characterization; spider silk; X-ray diffraction; infrared spectroscopy.

ABSTRACT

Tubuliform silk glands were dissected from *Nephila clavipes* spiders and silk gut fibers were produced by immersing the glands in a mild acid solution and subsequent stretching. The tensile properties of the as produced fibers were obtained through tensile tests and the stress-strain curves were compared with those of naturally spun tubuliform silk fibers. The influence on the mechanical properties of the fibers after immersion in water and drying was also discerned. The microstructure of the silk guts was obtained by X ray diffraction (XRD) and infrared spectroscopy (FTIR). It was found that the stress-strain curves of stretched tubuliform silk guts concur with their natural counterparts (tubuliform silk fibers).

I. INTRODUCTION

The formation and characterization of silk guts has proven a powerful tool for increasing our understanding on diverse silks in previous works [1, 2].Traditionally silkworm silk gut fibers were formed directly from the silk gland by immersion in a mild acid solution and subsequent stretching. This process was well known since the 18th century and used for producing the so-called "hijuelas" [3, 4]or "crins de Florence"[5] in several Mediterranean regions, such as in the southeastern coast of Spain (Región de Murcia), until the 1950s.

In this context, the study of the tubuliform (Tub) silk guts, which is undertaken for the first time in this work, tries to deal with the following questions regarding (1) the possible conservation of the spinning process characteristic of other spider and silkworm silk glands in the tubuliform gland, in spite of the large differences in sequences and the diversification of spinning glands, (2) the possible concurrence of the tensile properties of the silk gut and the naturally spun tubuliform fibers, and (3) a detailed microstructural characterization of the Tub silk guts under less demanding conditions than those required for the characterization of the naturally spun Tub fibers.

Spider silk is a unique example in Biology in which the production of a material is established as an essential trait that defines the clade of the spinning organisms[6]. In effect, one of the distinctive traits of the members of the *Araneae* clade, that distinguishes this group from other related lineages, is the capacity of producing silk fibers from specialized glands [6, 7]. In this regard, since the first appearance of the clade in the Devonian period[8], the evolution of the material explains much of the evolutionary success of the group and its ability to occupy a wide range of different ecological niches[9-11].

The comparison of spider silks spun by different species shows that the evolution of spider silk has proceeded in two main directions. Firstly, the molecular analysis shows that the silk proteins (spidroins) evolved from the archetypal molecules with several repetitions of the $-A_n-$ motif in their sequences [10] to more diversified sequences with the inclusion of new motifs, such as –GPG– and –GGX– [12, 13]. This scheme is specially recognizable in the major ampullate gland silk (MAS) of orb-web spiders [12] and contributes to the unrivalled toughness characteristic of these fibers [14].

Secondly, the ancestral silk gland diversified in different lineages to yield the seven different glands that are identified in the Orbicularians (orb-web spiders) [15]. This diversification has the immediate biological function of allowing the spider to adapt the properties of the material to different intended functions, such as building the structure of the web or swathing the prey [7]. Although it is usually assumed that the diversification of the silk glands did not modify the basic principles of the spinning mechanism [16] there are few direct evidences of this assertion.

Among the different silks produced by orb-web spiders, tubuliform (Tub) silk is used to build the inner cover of the ootheca to protect the offspring until hatching [15]. The characterization of Tub silk has revealed a number of intriguing features. Thus, the sequence of Tub spidroin is characterized by the absence of short repeats common in other silk proteins [17]. In contrast, a number of long and complex repeats rich in the amino acids alanine and serine, and with a low content of glycine, were found. In addition, previous microstructural characterizations of the Tub fibers did not identified the β-nanocrystals characteristic of silkworm and MAS silks [18, 19] In contrast a novel phase, known as twisted β-sheet, was proposed [20-22] which, although establishes the existence of a certain short-range order organization, depicts the corresponding twisted β-sheets as distorted nanocrystals subjected to a torsional deformation between their upper and lower faces [21]. However, the identification of the twisted β-sheet was based on transmission electron microscopy data due to the difficulties of performing accurate X-ray diffraction measurements on natural Tub fibers. In this regard, a similar uncertainty on the semicrystalline character of flagelliform silk (Flag) existed until an adequate preparation procedure, and the usage of a microdiffraction device and synchroton radiation allowed the identification of the nanocrystals in these fibers [23]. Consequently, the absence of clear X ray diffraction spots from the previous analysis on natural Tub fibers cannot be considered as a definitive evidence of the absence of long range organization in Tub silk. The purpose of this research is also to provide additional information on those aforementioned topics.

II. EXPERIMENTAL WORK

Preparation of *Nephila clavipes* tubuliform silk gut

Nephila clavipes (Linnaeus, 1767) spiders were reared in captivity in the facilities of Reptilmadrid S.L. (Madrid, Spain). Spiders were fed a diet of *Drosophila* flies for the 2-3 first moulds and of *Musca* flies from the 4th mould on. Adult females were used in this study. Prior to the dissection of the glands, spiders were anaesthetized with ethyl acetate. The tubuliform glands appear in two pairs of three glands each and are placed symmetrically at both sides of the anteroposterior plane and approximately in the middle region of the opistosome. In this species tubuliform silk glands show an elongated shape and are of an orange-yellowish colour. As explained below, the initial anatomical identification of the tubuliform glands was confirmed subsequently by protein analysis.

Upon retrieval the glands were kept in Ringer's solution for a period no longer than 30 minutes before starting the procedure for forming the silk gut. Based on previous works on silkworm silk gut [2, 24] and major ampullate gland silk gut [1], tubuliform glands were immersed in a 1% acetic acid solution in distilled water for 1 minute. Subsequently, the glands were removed from the solution, dried gently to remove the excess of liquid and stretched by hand.

Protein analysis

Glands used for protein analysis were frozen at -80 ºC immediately after being dissected and kept under this condition until starting the protein analysis protocol. Glands were later washed with cold PBS and each gland was immersed in 120 µl of homogenization buffer (50 mM Tris-HCl, pH 6.8, 10 mM DTT, 4% (w/v) SDS). Glands were boiled for 5 min, incubated at 4 ºC overnight and centrifuged 10 min at 4ºC and 13000 rpm for protein extraction. Samples were applied onto a conventional SDS-PAGE gel (0.5 mm-thick, 4% stacking, and 10% resolving). The run was stopped as soon as the front entered 2 mm into the resolving gel, so that the whole gland proteome became concentrated in the stacking/resolving gel interface [25]. The unseparated protein bands were visualized by Coomassie staining, excised and digested overnight at 37ºC with 500 µl of 25 µg/µl quimotrypsin (Promega) in 100 mM Tris-HCl, pH 7.8 containing 10 mM $CaCl_2$. The resulting peptides were extracted by 2h incubation in 100 mM Tris-HCl, pH 7.8 on shaking, acidized adding 1% (v/v) trifluoroacetic acid, desalted onto C18 cartridges (Oasis, Waters Corporation, Milford, MA, USA), and dried down.

Samples were analysed by NLC-/MS/MS using a Easy nLC 1000 coupled to a Q-Exactive Orbitrap mass spectrometer (Thermo Scientific). Peptides were loaded onto a C18 precolumn (Acclaim PepMap100, 75-µm i.d., 3-µm particle size, 2-cm length, Thermo Scientific), and separated on an analytical column (Acclaim PepMap 100, 75-µm i.d., 3-µm particle size, 50-cm length, Thermo Scientific) in a continuous gradient (10-30%B for 30 min), using HPLC buffers A (0.1% formic acid in HPLC H_2O) and B (80% ACN, 0.1% formic acid in HPLC grade H_2O) at 200 nl/min. Spectra with a FT resolution of 70000 were recorded in the mass interval m/z: 390-1200, followed by MS/MS spectra on the 15 parental ions of higher intensity. The higher-energy collisional dissociation (HCD) was fixed to 27% and the isolation window for the ion mass was 2 Da.

The sequencing of the peptides from the MS/MS spectra was performed with the SEQUEST HT algorithm implemented in Proteome Discoverer 2.1 (Thermo Scientific). The results of the MS/MS were compared with the database of *Aranae* proteins (UniProt 2016_10 Release). The searching parameters were selected under the following constraints: quimotrypsin digestion allowing for 2 maximum loss cleavages, tolerance of the mass of the precursor 20 ppm and tolerance of the mass of the fragment 0.02 ppm. The carbamidomethylation of cysteine was taken as fixed modification, while the oxidation of methionine was chosen as dynamic modification. The same collections of the MS/MS spectra were registered in inverted databases built from the same target databases. SEQUEST results were analysed with the method of "reason of probability" [26]. The false discovery rate (FDR) was calculated for the peptides identified in the results of the search in the inverted database by using the refined method [27]. Spectral counting was performed to calculate the proportion of proteins identified in the gland, considering only proteins identified in two replicates with more than one peptide in at least one of the two replicates at 1% FDR.

Mechanical characterization

Stretched silk guts were mounted on aluminium foil frames with a gauge length of 10 mm as explained elsewhere [28]. This gauge length was selected in order to maximize the number of retrieved samples that could be used for the different mechanical and microstructural characterization techniques, while maintaining a sufficient precision in the measurement of the initial length to yield accurate values of strain during tensile

testing. Micrographs were obtained with an OPTEM Zoom 125 camera and the apparent diameter of the fibers was measured from these micrographs using the ImageJ program. The cross-sectional area was calculated from the apparent diameter by assuming a circular cross section.

The aluminium foil frames were fixed to the grips of a tensile testing Instron machine 4411 (Resolution ±10 μm). The lower grip rested on a balance KERN PLJ (Resolution ±10 mgf) used to measure the force, F, exerted on the fiber [28]. Tensile tests proceeded at a speed of 1 mm/min under nominal environmental conditions T=23 ºC and RH=30%.

Engineering strain, e, and stress, s, were calculated as:

$$e = \frac{\Delta L}{L_0} \quad ; \quad s = \frac{F}{A_0} \qquad (1)$$

Where ΔL is the displacement of the upper grip of the tensile testing machine, since the compliance of the fiber was estimated as 1000-fold higher than that of the rest of the experimental setup [28]; L_0 is the initial length of the fiber, and A_0 is the initial cross sectional area of the fiber.

True strain, ε, and true stress, σ, were calculated from the engineering magnitudes under the hypothesis of constant volume, proved to be valid for natural major ampullate gland silk [29], as:

$$\varepsilon = Ln(1+e) \quad ; \quad \sigma = s(1+e) \qquad (2)$$

Some stretched silk guts were allowed to contract in water as explained elsewhere [30]. Samples were immersed in water for 30 minutes and allowed to dry overnight before being tested. The possible contraction was determined by comparing the zero load length of the fiber (i.e. the length at which the load on the fiber is zero, but the fiber is fully extended along a straight line) before and after being immersed in water and dried. Samples subjected to immersion in water and drying are labelled as Iw.

Microstructural characterization

The microstructure of the silk guts was analysed by infrared spectroscopy and X ray diffraction. Non-polarized infrared spectra were obtained by using a Nicolet iS5 spectrometer equipped with an iD5 ATR complement, as described elsewhere [31]. The area scanned with the spectrometer was ~ 1 mm^2 and spectra were determined as the average of 64 measurements in the range 550-4000 cm^{-1} (resolution 4 cm^{-1}). The amide I peak (1580-1700 cm^{-1}) was fitted to Gaussian functions. All the fitting process was performed with the Omnic 9 software. The assignment of the elementary contributions to the amide I peak was performed by following previous works [32] and is indicated in **Table 1**.

Wavenumber (cm^{-1})	Assignment
1594-1609	Tyr side chain/aggregated strand
1610-1620	Aggregate strand/intermolecular β sheet
1621-1627	Intermolecular β sheet
1628-1637	Intramolecular β sheet
1638-1655	Random coil
1656-1662	Helical structures
1663-1694	β-turn
1696-1703	Intermolecular β-sheet

Table 1. Assignment of the elementary contributions in the amide I region.

X ray diffraction patterns were obtained with a single crystal CCD Bruker AXS Smart 1000 diffractometer on a scanning area of ~0.25 mm^2. Molybdenum K-α radiation (λ=0.71 Å) was employed. Specimens were subjected to a 360 s exposure. A background image was acquired under the same conditions. The analysed images were obtained after substracting the background from the original image. The data analysis program FIT2D was used for calibration (Si pattern) and for image integration.

III. RESULTS

The anatomical identification of the glands used for the fabrication of the silk gut was supported by sequencing the proteins of the dope. The peptides identified by mass spectroscopy are listed in **Table 2**, where the peptides are presented in two groups labelled as *Q3BCG2_NEPCL Tubuliform spidroin* and *O17434_NEPCL Minor ampullate silk protein MiSp1*. The code indicates whether the peptide is present in the sequence of *Nephila clavipes* tubuliform spidroin (Tub, Q3BCG2_NEPCL) or in the sequence of the *N. clavipes* minor ampullate gland spidroin 1 (miS, O174334_NEPCL). The proportion of each protein calculated by spectral counting showed that peptides or *Tubuliform spidroin* represented 22% and peptides of *Minor ampullate silk protein MiSp1* represented 4% of the whole gland proteome, being the last one 1/6 of the characteristic tubuliform silk gland protein (**Figure 1**). The presence of peptides corresponding to miS spidroin in the dope of the tubuliform glands was totally unexpected from previous studies and its possible significance will be discussed below.

Q3BCG2_NEPCL Tubuliform spidroin
ARAVGALGQGATAASY
ARAAGALGQGATAASY
GIADAAGLAGAL
SAARSLGIADAAGL
APANAQIIAPGLQTTL
GNALSTAAGQF
SSASANARVSSL
AGALARAAGAL
AGALARAVGAL
SAARSLGIADATGL
APANAQIIAPGL
AQAASSSLATSSAL
QQAASRSASQSAAEAGSTSSSTTTTTSAARSQAASQSASSSY
SIGISAARSLGIADAAGL

O17434_NEPCL Minor ampullate silk protein
GRGAGAGAGAAAGAGAGAAAGAGAGAGGY
GAGAGAAAAAGAGAGGAGGY
GAGAGAGAAAAAGAGAGGAAGY
GAGAGAGAAAAAGAGAGGAGGY
GAGAGAGAAAAAGAGAGGY
GRGAGAGAGAAAGAGAGAAAGAGAGGY
GRGAGAGAGAAAGAGAGAGGY
GRGAGAGAGAAAGAGAGGY
GRGAGAGAGAAAGAGAGAGGAGY
GRGAGAGAGAAAGAGAGTGGAGY

Table 2. Peptide sequences identified by mass spectrometry in the protein extract of the tubuliform gland. The labels Q3BCG2_NEPCL Tubuliform spidroin and O17434_NEPCL Minor ampullate silk protein indicate the presence of the peptide in the corresponding protein sequence.

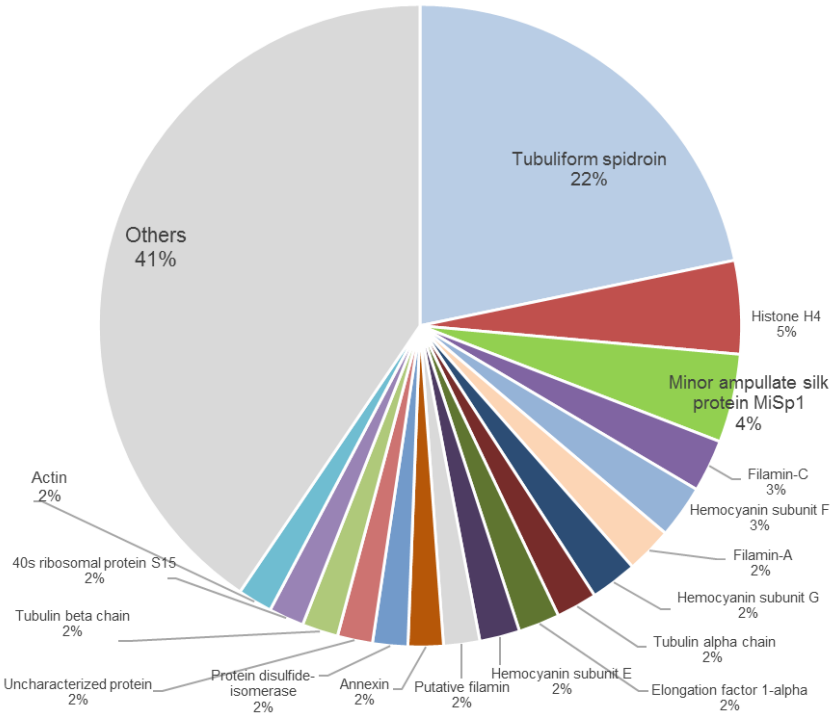

Figure 1. Quantitative proteome of *Nephila clavipes* tubuliform gland. Protein composition showed and unexpected high proportion of minor ampullate silk protein MiSp1 in the tubuliform gland proteome. The proportion of the proteins identified by mass spectrometry was calculated by spectral counting, considering proteins identified in two replicates and with more than 1 peptide in at least one of the replicates at 1% FDR. "Others" symbolizes a group of proteins that represent individually a proportion of <1.5% in the proteome.

Stretched silk guts were produced, as explained above, by immersing the tubuliform glands in a 1 % acetic acid solution for 1 minute and, subsequently, stretching the gland by hand. Typically, fibers with a length of approximately 150 mm and diameters in the range between 15 μm and 130 μm were produced by using this procedure. Variations of approximately 100 % in the values of the diameter were recorded from micrographs corresponding to different regions of the same silk gut. Following previous works [1, 2], stresses were calculated using the minimum value of the diameter of the silk gut. This way the calculated values of tensile strength are accurate, although the values of strain in the stress-strain curve may be underestimated. Representative micrographs of silk guts obtained at the same magnification, that illustrate the range of diameters, are shown in **Figure 2**.

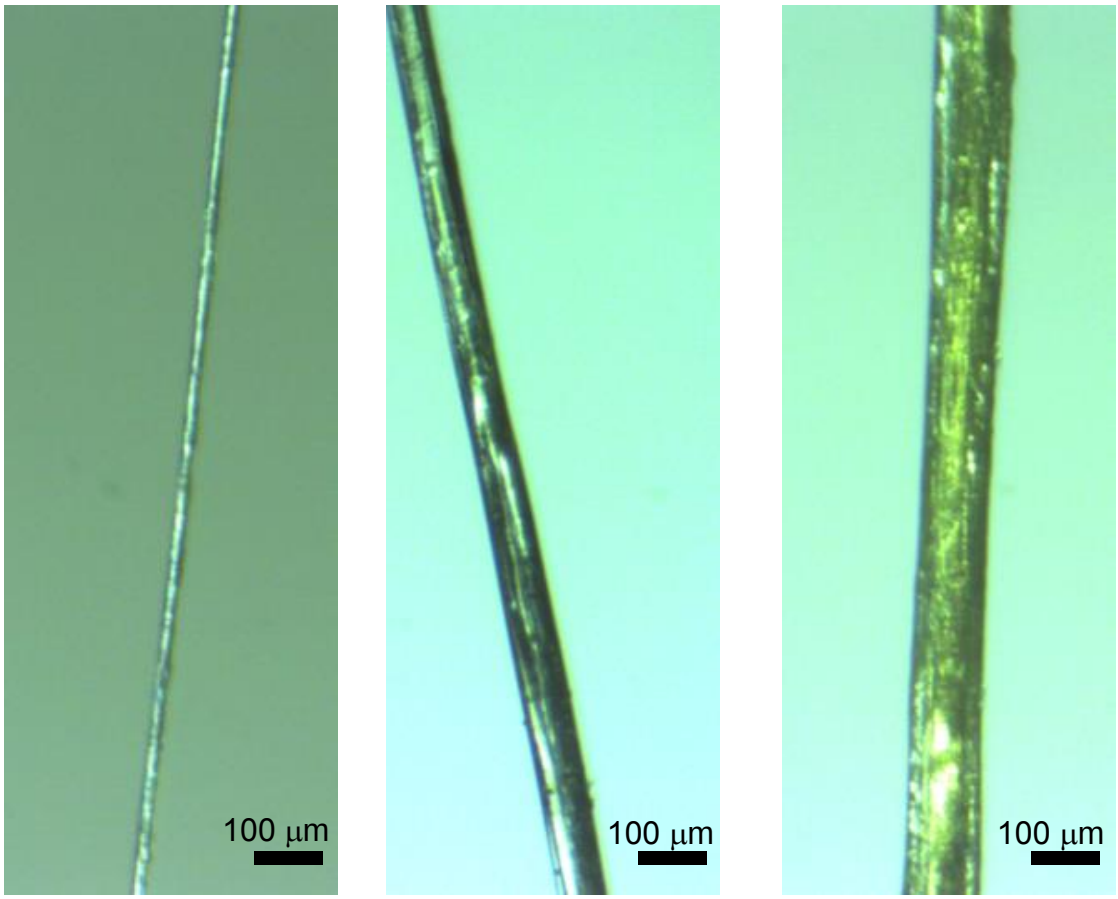

Figure 2. Micrographs of different tubulliform silk guts produced by immersion in a 1 % acetic acid solution for 1 minute and subsequent stretching by hand.

The tensile properties of the tubuliform silk guts are shown in **Figure 3**. The true stress-true strain curves of tubuliform silk guts as prepared and tested in air are shown in **Figure 3a**. A relatively large variability in the tensile properties is observed as found previously with other silk guts [1, 2]. The maximum values measured for tensile strength and strain at breaking were 376 MPa and 0.18, respectively, which yields a remarkable value for the work to fracture of ~40 MJ/m^3. **Figure 3b** compares the true stress-true strain curves of *N. clavipes* tubuliform silk gut, with the true stress-true strain curves of naturally spun *Argiope argentata* [15] and *Argiope bruennichi* [33] tubuliform silks. Except for the reduced tensile strength of the tubuliform silk gut, all tubuliform fibers show concurring tensile properties, in spite of being produced by spiders that diverged over 120 Mya ago [34]. In spite of the concurring tensile properties in terms of stress, **Figure 3c** highlights the enormous difference in terms of force when the tubuliform silk guts, that can reach loads up to 600 mN, are compared with naturally spun tubuliform fibers [33].

The analysis of the effects exerted by water on the tensile properties of silks is a powerful tool for exploring the relationship between microstructure and mechanical behaviour in these materials [35]. For instance, the discovery of supercontraction in the major ampullate gland silk of orb-weaving spiders [36] was exploited not only to establish the mechanisms that underlie the tensile properties of spider silk [37], but also for comparing the tensile properties of silk fibers spun by different spider species [38]. Following this rationale, tubuliform silk guts were immersed in water under conditions that allowed their contraction, dried and tensile tested until breaking. The comparison of the length of the fibers before and after being immersed in water and allowed to contract did not reveal any change in the dimensions of the fiber within the precision of the experimental setup. A similar absence of supercontraction in natural tubuliform fibers had been also reported [33].

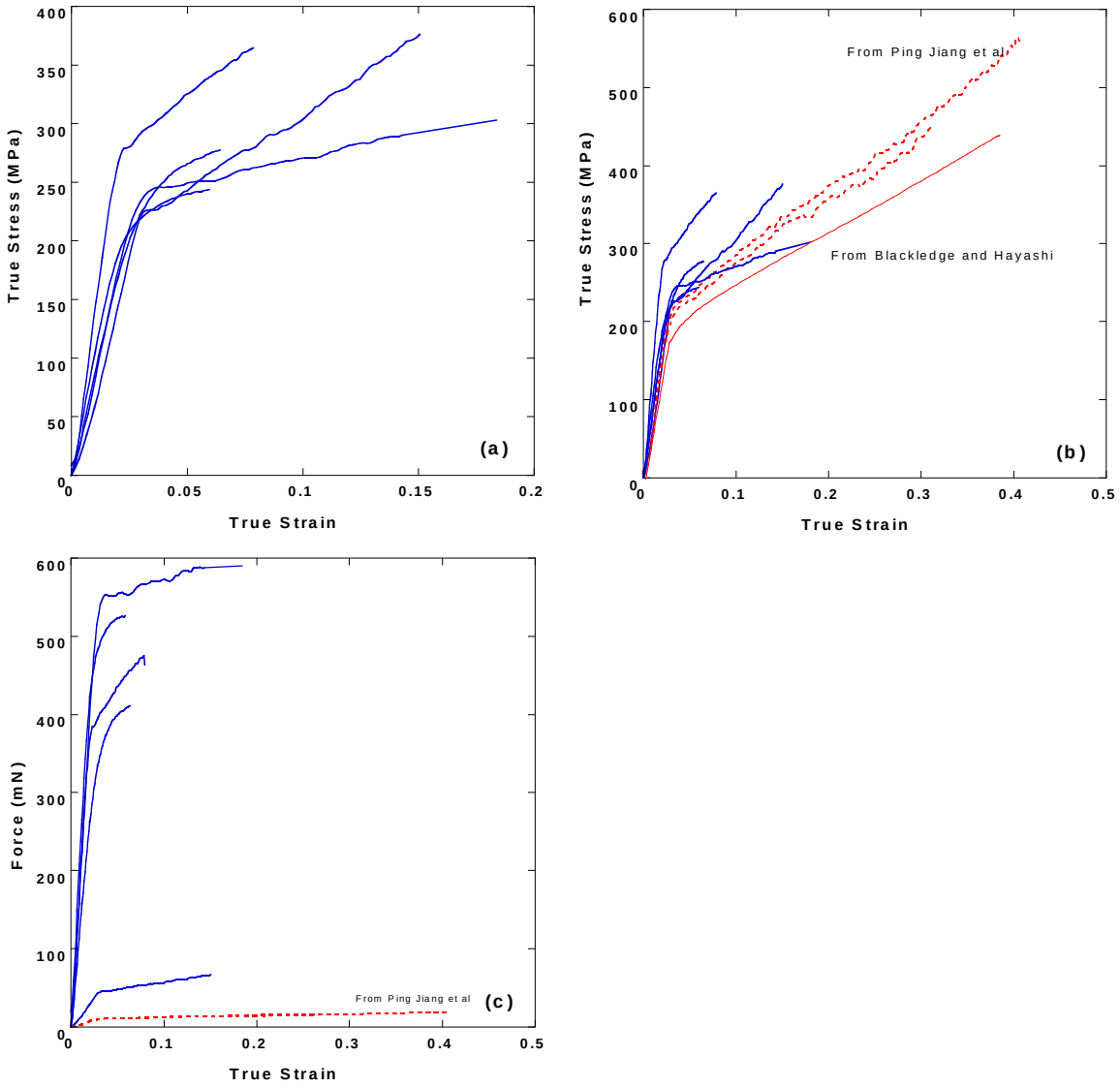

Figure 3. Tensile properties of tubuliform silk guts. (a) True stress-true strain curves of tubuliform silk guts as prepared and tested in air. (b) Comparison of the true stress-true strain curves of *Nephila clavipes* tubuliform silk guts and naturally spun tubuliform silk spun by *Argiope argentata* [15] and by *Argiope bruennichi* [33]. (c) Comparison of the force-true strain curves of *N. clavipes* tubuliform silk guts and *A. bruennichi* naturally spun tubuliform fibers (broken line) [33].

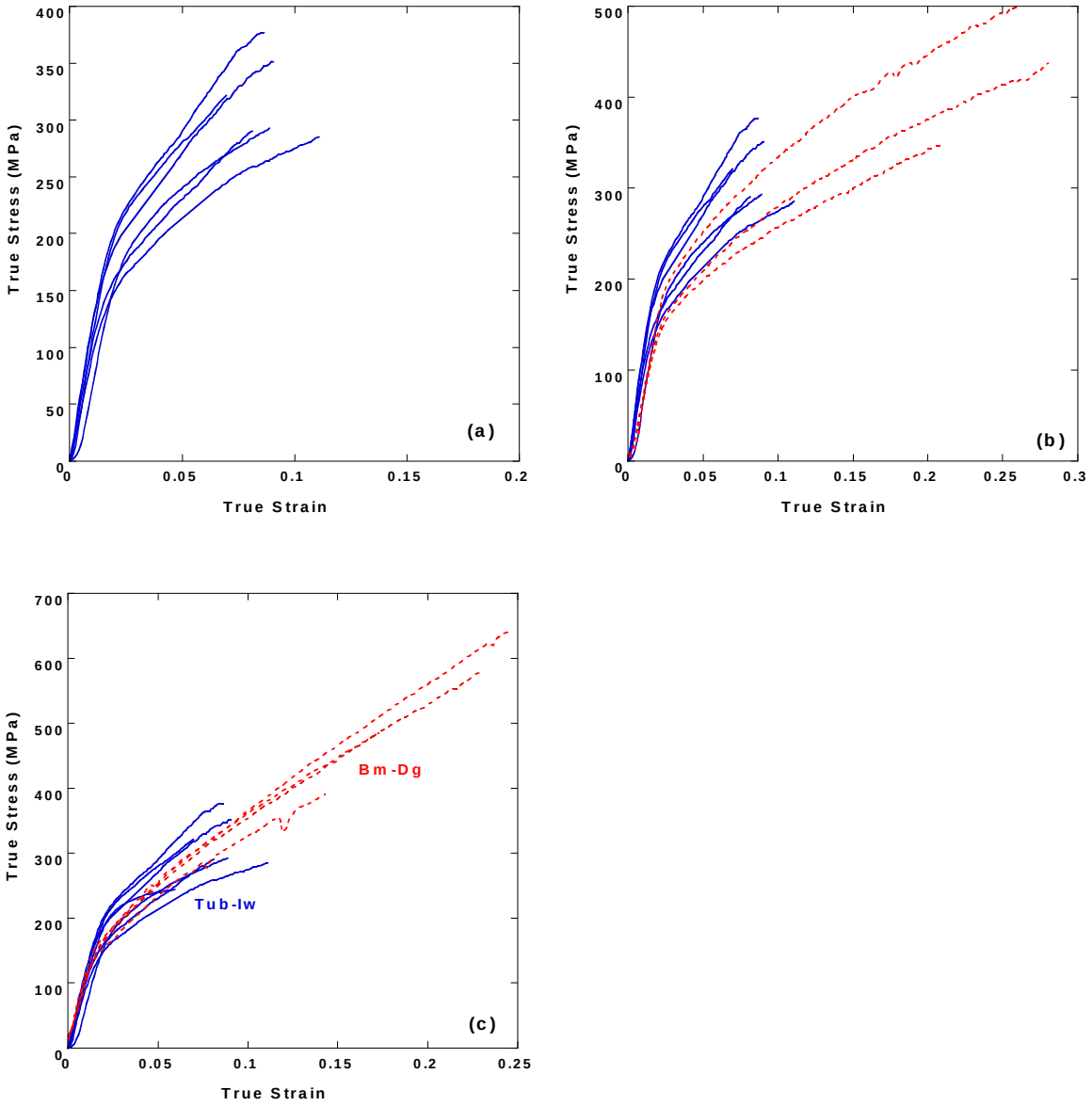

Figure 4. Tensile properties of tubuliform silk guts after being immersed in water for 30 minutes and dried overnight. (a) True stress-true strain curves of tubuliform silk guts tested in air. (b) Comparison of the true stress-true strain curves of *Nephila clavipes* tubuliform silk guts and naturally spun tubuliform silk spun by *Argiope bruennichi*. Both sets of fibers were immersed in water, allowed to contract and dried before being tested

[33]. (c) Comparison of the true stress-true strain curves of tubuliform silk gut (Tub-Iw) and degummed silkworm silk fibers (Bm-Dg) [39].

The tensile properties of tubuliform silk guts after immersion in water and drying are shown in **Figure 4a**. After being immersed in water and dried silk guts show more reproducible tensile properties in terms of true stress-true stress curves, compared with the data shown in **Figure 3a**. Although the silk guts after immersion yield values of tensile strength comparable to those of the as-prepared material, the maximum values of strain at breaking are significantly reduced. This reduction in the maximum values of strain at breaking implies that after being immersed and dried, the silk gut fibers reach a maximum value of work to fracture of W_f~20 MJ/m^3. **Figure 4b** shows the comparison of silk guts and naturally spun tubuliform silk spun by *A. bruennichi* after being subjected to the same process of immersion in water for 30 minutes and being dried overnight [33]. As also observed in **Figure 4b**, both silk guts and naturally spun tubuliform silk fibers show concurring true stress-true strain properties, except for the reduction in the tensile strength observed in the former. In addition, in **Figure 4c** the remarkable concurring tensile behaviour (except again for the differing values of tensile strength) of tubuliform silk gut and degummed silkworm silk [39] is shown.

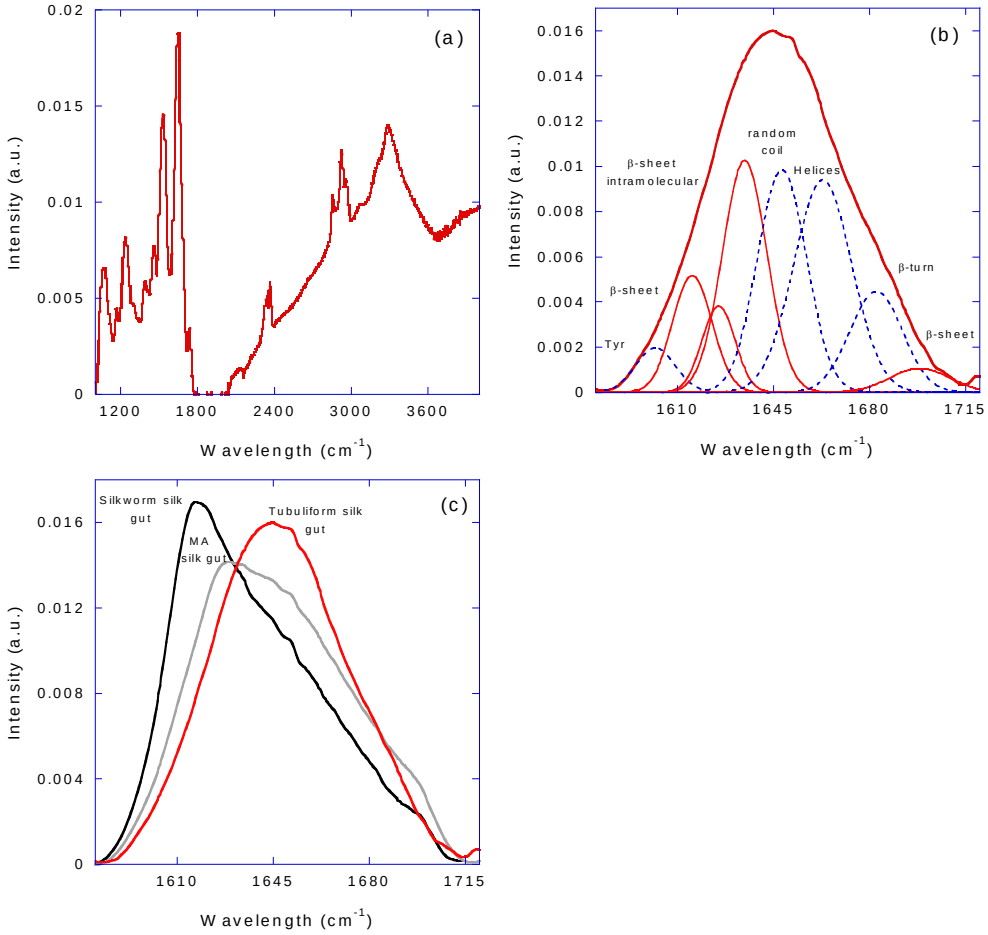

Figure 5. Microstructural characterization of tubuliform silk gut: Infrared spectroscopy. (a) Representative FTIR-ATR spectrum of a tubuliform silk gut fiber. (b) Detail of the amide I peak of a representative FTIR-ATR spectrum of tubuliform silk gut. The elementary contributions to the amide I peak are indicated following the assigments of **Table 1**. (c) Comparison of the Amide I peaks of tubuliform silk gut, silkworm silk gut and major ampullate gland silk gut.

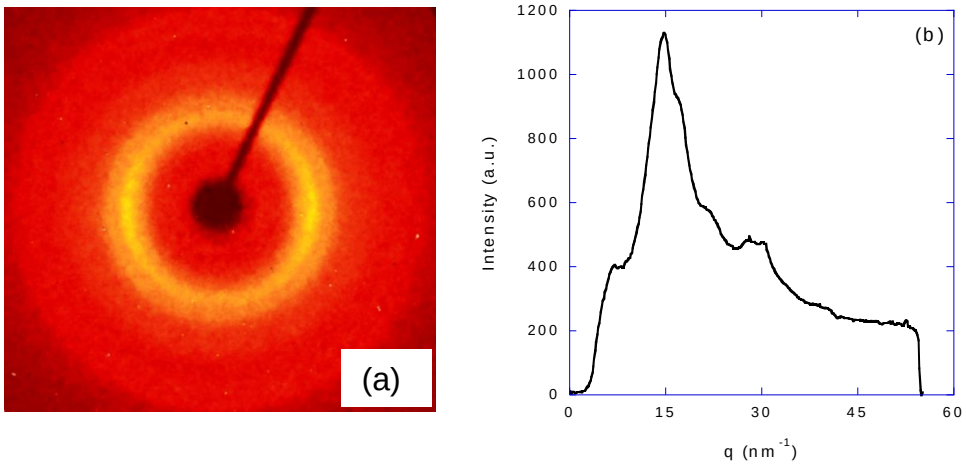

Figure 6. Microstructural characterization of tubuliform silk gut: X ray diffraction. (a) Representative X ray diffraction pattern of a tubuliform silk gut. (b) X ray diffraction intensity vs. the length of the reciprocal vector, q, obtained by azimuthal integration of the X ray diffraction pattern.

The mechanical characterization of tubuliform silk gut was completed with a microstructural analysis performed by using FTIR and XRD. **Figure 5** summarizes the main results obtained from the FTIR characterization. **Figure 5a** shows a representative FTIR spectrum in which the different vibrational modes of the tubuliform silk gut can be identified. In particular the signal recorded in the region between 1750 cm^{-1} and 2650 cm^{-1} indicates the presence of absorbed water molecules in the fiber, as found in previous works on natural silkworm silk[40]. Although the presence of absorbed water molecules may modify the intensity in other regions of the spectrum, these changes were shown to decrease significantly and finally to stabilize after a period of approximately 30 minutes[40], much shorter than the times spanned between the formation of the tubuliform silk gut and its FTIR characterization in this work.

Following the common procedure for the analysis of FTIR data from silk fibers[41], the analysis concentrated on the Amide I peak ranging from 1580 cm^{-1} to 1720 cm^{-1} (**Figure 5b**). The deconvolution into elementary gaussian functions shown in **Figure 5b** is employed conventionally to assess the relative abundance of each secondary structure in the fiber. The assignment of the different Gaussian functions to the various elementary contributions was made following **Table 1**.

Finally, the amide I peak of the tubuliform silk gut is compared with the corresponding amide I peaks of major ampullate gland silk gut [1] and silkworm silk gut [2] in **Figure 5c**. The variation in the position of the amide I peak between the three fibers reflects differences in their microstructures. Although, as explained above, the presence of absorbed water might modify the FTIR intensity in this region, the similar observation conditions employed for all three samples preclude that the observed differences might be an artifact arising from different water contents.

In an attempt to identify the possible existence of a crystalline phase in tubuliform silk gut, X ray diffraction patterns were recorded from these fibers as illustrated in **Figure 6a**. The X ray diffraction intensity as a function of the reciprocal wavevector, q, obtained through the azimuthal integration of the diffractogram is presented in **Figure 6b**. The presence of diffraction spots is evident in **Figure 6a**, and the XRD intensity vs. q plot allows identifying two main contributions at q_1=14.7 nm^{-1} and q_2=16.7 nm^{-1}. These diffraction peaks are shown to coincide with those of the (210) and (002) crystallographic planes previously described in *Argiope trifasciata* minor ampullate gland silk[42], which suggests that the nanocrystals in both types of fibers share a common unit cell.

IV. DISCUSSION

It may be worth emphasizing that one of the basic results presented above is the verification that fibers can be obtained directly from the tubuliform silk glands by such a simple procedure as immersing the gland in a mild acid solution and stretching it. Such a procedure was found to lead to the production of fibers from silkworm silk glands [2] and spider major ampullate gland [1] but to the authors' best knowledge, it is the first time that silk guts are produced from spider tubuliform silk glands.

The possibility of producing tubuliform silk guts highlights again the two essential conditions required for spinning fibers from a spidroin or fibroin solution, namely the requirement of (1) exposing the proteins to a low pH environment and (2) of being subjected subsequently to mechanical stress that complete the transition from fluid to solid. The common principles required for producing fibers from the major ampullate and tubuliform glands indicate the conservation of the spinning mechanism in spite of the diversification of the spider's spinning glands [9, 43, 44]. Notably, a similar mechanism is also found in silkworm silk glands, although the appearance of silk glands in spiders and worms is thought to result from two independent evolutionary events [45]. In this regard, the influence of pH on the spinning process was initially proposed [46] and subsequently established after identifying the existence of pH-switches in fibroins [47, 48]. It is hypothesized that changes in pH induce the self-assembly of the fibroins, which makes them susceptible to the mechanical stresses that induce the transition from protein solution to a solid fiber [49, 50]. The results on tubuliform silk gut confim again that variations in the pH of the protein solution and mechanical stresses are not only necessary, but also the sufficient conditions for the production of silk fibers.

The comparison of tubuliform silk guts with those silk guts previously produced allows establishing a few more general principles shared by this type of fibers, although Tub silk gut shows some remarkable singularities. When compared with their natural counterparts (that is to say, the corresponding naturally spun silks), all silk guts show lower values of tensile strength and strain at breaking, a well known effect that might result from the inverse correlation between tensile strength and the diameter of the fiber [51]. At this point, however, a first difference can be established between spider (MAS or Tub) and silkworm silk guts when compared with the naturally spun fibers. In this regard, the stress-strain curves of spider silk guts are shown to concur with those of the naturally spun fibers up

to the breaking point of the former. In contrast, silkworm silk guts are more compliant than natural silkworm silk, an effect that seems to be related with lower values of crystallinity in the silk gut [2].

The similar properties exhibited by MA spider silk gut fibers and naturally spun fibers was shown to extend to the existence of supercontraction [36] in both types of fibers [1]. Supercontraction is exhibited by many, but not all, natural spider silk fibers. In particular, supercontraction was not observed in Tub silk fibers spun by *A. bruennichi* spiders [33]. The results presented on Tub silk guts from *N. clavipes* also establish the absence of supercontraction in these fibers. However, immersion in water is shown to induce some changes in the mechanical properties of Tub silk gut, as also observed in naturally spun silkworm silk [39], although none of these fibers do supercontract. Most remarkably, immersion in water leads to a significant increase in the reproducibility of the stress-strain curves of tubuliform silk gut fibers (see **Figure 4a**) which, in addition, are shown to concur with the stress-strain curves of *A. bruennichi* Tub silk upon being immersed in water and dried [33] (see **Figure 4b**).

Apart from supporting some previous conclusions obtained from the study of MA and silkworm silk guts, the mechanical and microstructural characterization of Tub silk gut renders some singular results on these fibers. In this regard, the presence of peptides characteristic of the minor ampullate silk spidroin in the tubuliform gland can be considered as a largely unexpected result. The characteristic sequence of tubuliform silk as found in previous works corresponds to the *Tubuliform spidroin* column in **Table 2** [17, 52, 53]. However, the analysis of the proteins characteristic of the tubuliform gland in previous studies relied on the construction of cDNA libraries, so that the possible expression of other spidroins in the tubuliform gland was not considered and could not be detected. At this stage the identification of miSp peptides in the tubuliform gland opens a number of questions that will require further work to be solved.

To begin with, the label “miSp-like spidroin” used above refers to the uncertainty on the gene encoding for this protein. From the present data, it might be encoded by the same gene that encodes the well-known miSp spidroin which, in addition to its expression in the minor ampullate gland, would be also expressed in the tubuliform gland. However, it cannot be discarded that a different gene might be responsible for encoding the protein

produced in the tubuliform gland. Independently from the discussion on the gene that encodes this protein, the relevance of the miSp-like spidroin is highlighted by the quantitative proportion 6:1 Tub : miSp-like between both spidroins, and further stressed by the presence of a crystalline phase in the fibers with the same unit cell as that found in naturally spun minor ampullate gland silk fibers.

In spite of the uncertainties related to the presence of the miSp-like spidroin in the gland, the analysis of tubuliform spidroins with sequences similar to that of Q3BCG2_NEPCL in previous works showed their conservation in different spider species such as *Argiope aurantia, Araneus gemmoides* and *Nephila clavipes* [52]. The results on the mechanical characterization of Tub silk gut indicates that the conserved traits among Tub silk spun by different species extend to the properties of the silk gut. Thus, *N. clavipes* tubuliform silk gut is shown to yield concurring tensile properties with those of the naturally spun Tub silks spun by *A. argentata* and *A. bruennichi* spiders. The extreme conservation of the tensile properties of Tub silk contrasts with the results obtained for MAS fibers, in which large variations in the stress-strain curves of fibers spun by different species are found [38, 54].

There is finally another intriguing property of tubuliform silk that is highlighted by the previous results. As presented in **Figure 4c** the stress-strain curves of tubuliform silk gut concur with those of degummed silkworm silk, in particular both types of fibers yield comparable values of the initial elastic modulus (E~10 GPa). The large value of the elastic modulus in silkworm silk is usually considered as a direct consequence of the high crystallinity of these fibers [19]. However, the compositional analysis of the tubuliform silk gut reveals that only approximately 1/6 of the protein content corresponds to the miSp-like spidroin, whose presence justifies the formation of the nanocrystalline phase observed by XRD. In addition, a low crystallinity of tubuliform silk gut is further supported by the reduced content in β-sheet secondary structure, as shown from the deconvolution of the amide I peak recorded in the FTIR spectra, and by the displacement of the amide I with respect to that measured from silkworm and MA spider silk guts.

The apparent mismatch between the microstructural data and the mechanical characterization supports the previously stated hypothesis that naturally Tub silk contains a different type of short-range microstructural motifs named as β-sheet twists [20, 21], that

differ from the usual β-nanocrystals [55]. These microstructural motifs would appear in the transition of the fully amorphous state of silk in the gland [5, 41] to the solid fiber, and might be inhomogeneously distributed in the fiber[56]. In this case, the spatial resolution of the microstructural techniques employed would not allow the assessment of the possible inhomogeneities in the distribution of the various microstructural motifs described above. It is intriguing, however, how the presence of the tubuliform spidroin may contribute to impart to the Tub silk the high values of elastic modulus characteristic of the highly crystalline silkworm silk fibers used to protect the pupa during the metamorphosis [39].

V. CONCLUSIONS

Silk guts can be produced from tubuliform silk glands of *N. clavipes* spiders by immersion of the glands in a mild acidified solution and subsequent stretching. Fibers with remarkable tensile properties are produced, whose stress-strain curves concur with those of the naturally spun tubuliform silk fibers. Silk gut fibers, however, show lower values of tensile strength and strain at breaking, although they outperform their natural counterparts when force and not stress is considered.

The comparison of the tensile properties of *N. clavipes* silk gut fibers with tubuliform fibers naturally spun by other species also shows the extreme conservation of the mechanical performance of these fibers. The stability in the properties of these fibers was suggested by the conservation of the tubuliform spidroin sequences even in distant species considered in evolutionary terms.

The proteomic analysis of *N. clavipes* tubuliform glands has revealed the presence of a miSp-like protein in the gland. The role of this protein seems to be the formation of a nanocrystalline phase with a unit cell similar to that found in minor ampullate gland silk fibers.

Finally, the role of the majority tubuliform spidroin remains an intriguing question. In particular, future works will have to address the possible influence of this protein in the high elastic modulus of tubuliform silk gut. In this regard, the existence of short-range structures named as β-sheet twist might be a possible explanation to reconcile the relatively low crystallinity of tubuliform fibers with values of the elastic modulus found in much more crystalline silk fibers, such as silkworm silk.

AUTHORS CONTRIBUTIONS

VR and PJ retrieved the glands, produced the silk guts and performed the mechanical characterizacion with the help of CM, ME and GVG. CM performed the FTIR measurements and analysis. IJ and JV performed the proteomic analysis. AR was responsible for the XRD measurements. SDA-C, JLC and LM-O helped in the preparation of the silk guts. JPR coordinated the experimental work and wrote the main text. All authors contributed to the data analysis and reviewed the manuscript.

CONFLICT OF INTEREST

There are no conflicts of interest to declare.

ACKNOWLEDGEMENTS

Spiders were reared in Reptilmadrid S.L. by Oscar Campos. The work was funded by the Ministry of Economy and Competitiveness in Spain through projects MAT2016-75544-C2 and MAT2016-79832-R, and from Comunidad de Madrid (Spain) through grant NEUROCENTRO-B2017/BMD-3760. Dr. Salvador D. Aznar-Cervantes acknowledges the financial support of this research contract, program INIA-CCAA (DOC INIA 2015), announced by the National Institute for Agricultural and Food Research and Technology (INIA) and supported by the Spanish State Research Agency (AEI) under the Spanish Ministry of Economy, Industry and Competitiveness. Dr. Ping Jiang acknowledges financial support from the National Natural Sciences Foundation of China (No.30760041; No.31160420), the education department of Jiangxi province through Science and technology projects (No.GJJ170626), the Natural Sciences Foundation of Jiangxi province (No.20151BAB204019), the Training Program of Young Scientists (Jinggang Star) in Jiangxi Province (No.20133BCB23022) and the Special Fund for Visiting Scholar of the Development Plan for Middle-aged and Young Teachers in Universities of Jiangxi Province (No.2016109). This study was also supported by competitive grants from the Spanish Ministry of Economy and Competitiveness (MINECO) (BIO2015-67580-P) through the Carlos III Institute of Health-Fondo de Investigación Sanitaria (PRB2, IPT13/0001 - ISCIII-SGEFI/FEDER, ProteoRed), and by CIBERCV (CB16/11/00277). The CNIC is supported by the MINECO and the Pro-CNIC Foundation, and is a Severo Ochoa Center of Excellence (MINECO award SEV-2015-0505).

REFERENCES

1 P. Jiang, N. Mari-Buye, R. Madurga, M. Arroyo-Hernandez, C. Solanas, A. Ganan, R. Daza, G. R. Plaza, G. V. Guinea, M. Elices, J. L. Cenis and J. Perez-Rigueiro, *Scientific Reports*, 2014, **4**, 7326 (DOI:10.1038/srep07326).

2 J. L. Cenis, R. Madurga, S. D. Aznar-Cervantes, A. Abel Lozano-Perez, N. Mari-Buye, L. Meseguer-Olmo, G. R. Plaza, G. V. Guinea, M. Elices, F. Del Pozo and J. Perez-Rigueiro, *Soft Matter*, 2015, **11**, 8981-8991 (DOI:10.1039/c5sm01877c).

3 A. M. C. Humphries, *Post Graduate Medical Journal*, 1949, **October**, 483-488.

4 L. Marden, *National Geographic Magazine*, 1951, **100**, 100-108.

5 P. Colomban, Hung Manh Dinh, A. Tournie and V. Jauzein, *J. Raman Spectrosc.*, 2012, **43**, 1042-1048 (DOI:10.1002/jrs.3122).

6 R. F. Foelix, *Biology of spiders*, Oxford University Press, Oxford, 2011.

7 F. Vollrath, *Sci. Am.*, 1992, **266**, 70-76.

8 P. A. Selden, W. A. Shear and M. D. Sutton, *Proc. Natl. Acad. Sci. U. S. A.*, 2008, **105**, 20781-20785 (DOI:10.1073/pnas.0809174106).

9 C. Y. Hayashi, N. H. Shipley and R. V. Lewis, *Int. J. Biol. Macromol.*, 1999, **24**, 271-275.

10 J. Gatesy, C. Hayashi, D. Motriuk, J. Woods and R. Lewis, *Science*, 2001, **291**, 2603-2605.

11 T. A. Blackledge, N. Scharff, J. A. Coddington, T. Szuts, J. W. Wenzel, C. Y. Hayashi and I. Agnarsson, *Proc. Natl. Acad. Sci. U. S. A.*, 2009, **106**, 5229-5234 (DOI:10.1073/pnas.0901377106 ER).

12 M. Xu and R. V. Lewis, *Proc. Natl. Acad. Sci. U. S. A.*, 1990, **87**, 7120-7124.

13 B. O. Swanson, T. A. Blackledge, A. P. Summers and C. Y. Hayashi, *Evolution*, 2006, **60**, 2539-2551.

14 M. Heim, D. Keerl and T. Scheibel, *Angew. Chem. Int. Ed Engl.*, 2009, **48**, 3584-96.

15 T. A. Blackledge and C. Y. Hayashi, *J. Exp. Biol.*, 2006, **209**, 2452-2461 (DOI:10.1242/jeb.02275 ER).

16 M. Andersson, J. Johansson and A. Rising, *International Journal of Molecular Sciences*, 2016, **17**, UNSP 1290 (DOI:10.3390/ijms17081290).

17 J. E. Garb and C. Y. Hayashi, *Proc. Natl. Acad. Sci. U. S. A.*, 2005, **102**, 11379-11384 (DOI:10.1073/pnas.0502473102 ER).

18 C. Riekel, C. Branden, C. Craig, C. Ferrero, F. Heidelbach and M. Muller, *Int. J. Biol. Macromol.*, 1999, **24**, 179-186.

19 A. Martel, M. Burghammer, R. J. Davies and C. Riekel, *Biomacromolecules*, 2007, **8**, 3548-3556 (DOI:10.1021/bm700935w ER).

20 J. Y. J. Barghout, B. L. Thiel and C. Viney, *Int. J. Biol. Macromol.*, 1999, **24**, 211-217 (DOI:10.1016/S0141-8130(99)00007-0).

21 J. Y. J. Barghout, J. T. Czernuszka and C. Viney, *Polymer*, 2001, **42**, 5797-5800 (DOI:10.1016/S0032-3861(00)00846-6).

22 C. Dicko, D. Knight, J. M. Kenney and F. Vollrath, *Biomacromolecules*, 2004, **5**, 2105-2115 (DOI:10.1021/bm034486y ER).

23 G. B. Perea, C. Riekel, G. V. Guinea, R. Madurga, R. Daza, M. Burghammer, C. Hayashi, M. Elices, G. R. Plaza and J. Perez-Rigueiro, *Scientific Reports*, 2013, , 1-6 (DOI:10.1038/srep03061).

24 J. Luis Cenis, S. D. Aznar-Cervantes, A. Abel Lozano-Perez, M. Rojo, J. Munoz, L. Meseguer-Olmo and A. Arenas, *International Journal of Molecular Sciences*, 2016, **17**, UNSP 1142 (DOI:10.3390/ijms17071142).

25 E. Bonzon-Kulichenko, F. Garcia-Marques, M. Trevisan-Herraz and J. Vazquez, *Journal of Proteome Research*, 2015, **14**, 700-710 (DOI:10.1021/pr5007284).

26 E. J. Hsieh, M. R. Hoopmann, B. MacLean and M. J. MacCoss, *Journal of Proteome Research*, 2010, **9**, 1138-1143 (DOI:10.1021/pr900816a).

27 P. Navarro and J. Vazquez, *Journal of Proteome Research*, 2009, **8**, 1792-1796 (DOI:10.1021/pr800362h).

28 J. Perez-Rigueiro, C. Viney, J. Llorca and M. Elices, *J Appl Polym Sci*, 1998, **70**, 2439-2447.

29 G. V. Guinea, J. Perez-Rigueiro, G. R. Plaza and M. Elices, *Biomacromolecules*, 2006, **7**, 2173-2177 (DOI:10.1021/bm060138v ER).

30 J. Perez-Rigueiro, M. Elices and G. V. Guinea, *Polymer*, 2003, **44**, 3733-3736 (DOI:10.1016/S0032-3861(03)00245-3 ER).

31 R. Madurga, A. M. Ganan-Calvo, G. R. Plaza, G. V. Guinea, M. Elices and J. Perez-Rigueiro, *Biomacromolecules*, 2017, **18**, 1127-1133 (DOI:10.1021/acs.biomac.6b01757).

32 R. Madurga, A. M. Ganan-Calvo, G. R. Plaza, G. V. Guinea, M. Elices and J. Perez-Rigueiro, *Green Chem.*, 2017, **19**, 3380-3389 (DOI:10.1039/c7gc01254c).

33 P. Jiang, L. Wu, X. Liao, W. Long, A. Wang and C. Guo, *Sichuan Journal of Zoology*, 2018, **37**, 556-562.

34 M. Elices, G. R. Plaza, M. A. Arnedo, J. Pérez-Rigueiro, F. G. Torres and G. V. Guinea, *Biomacromolecules*, 2009, **10**, 1904-1910.

35 J. M. Gosline, M. W. Denny and M. E. Demont, *Nature*, 1984, **309**, 551-552.

36 R. W. Work, *Text. Res. J.*, 1977, **47**, 650-662.

37 K. N. Savage, P. A. Guerette and J. M. Gosline, *Biomacromolecules*, 2004, **5**, 675-679 (DOI:10.1021/bm034270w ER).

38 R. Madurga, G. R. Plaza, T. A. Blackledge, G. V. Guinea, M. Elices and J. Perez-Rigueiro, *Scientific Reports*, 2016, **6**, 18991 (DOI:10.1038/srep18991).

39 G. Belen Perea, C. Solanas, N. Mari-Buye, R. Madurga, F. Agullo-Rueda, A. Muinelo, C. Riekel, M. Burghammer, I. Jorge, J. Vazquez, G. R. Plaza, A. L. Torres, F. del Pozo, G. V. Guinea, M. Elices, J. Luis Cenis and J. Perez-Rigueiro, *European Polymer Journal*, 2016, **78**, 129-140 (DOI:10.1016/j.eurpolymj.2016.03.012).

40 A. Percot, P. Colomban, C. Paris, H. M. Dinh, M. Wojcieszak and B. Mauchamp, *Vibrational Spectroscopy*, 2014, **73**, 79-89 (DOI:10.1016/j.vibspec.2014.05.004).

41 V. Jauzein and P. Colomban, *Types, structure and mechanical properties of silk*, 2009.

42 G. V. Guinea, M. Elices, G. R. Plaza, G. B. Perea, R. Daza, C. Riekel, F. Agullo-Rueda, C. Hayashi, Y. Zhao and J. Perez-Rigueiro, *Biomacromolecules*, 2012, **13** (DOI:10.1021/bm3004644).

43 J. E. Garb, N. A. Ayoub and C. Y. Hayashi, *Bmc Evolutionary Biology*, 2010, **10**, 243 (DOI:10.1186/1471-2148-10-243).

44 J. Starrett, J. E. Garb, A. Kuelbs, U. O. Azubuike and C. Y. Hayashi, *Plos One*, 2012, **7**, e38084 (DOI:10.1371/journal.pone.0038084).

45 C. L. Craig and C. Riekel, *Comparative Biochemistry and Physiology B-Biochemistry & Molecular Biology*, 2002, **133**, 493-507 (DOI:10.1016/S1096-4959(02)00095-7).

46 F. Vollrath, D. P. Knight and X. W. Hu, *Proceedings of the Royal Society of London Series B-Biological Sciences,* 1998, **265**, 817-820.

47 F. Hagn, L. Eisoldt, J. G. Hardy, C. Vendrely, M. Coles, T. Scheibel and H. Kessler, *Nature,* 2010, **465**, 239-242.

48 G. Askarieh, M. Hedhammar, K. Nordling, A. Saenz, C. Casals, A. Rising, J. Johansson and S. D. Knight, *Nature,* 2010, **465**, 236-239.

49 E. Iizuka, *Applied Polymer Symposia,* 1985, , 173-185.

50 C. Ortlepp and J. Gosline, *Biomacromolecules,* 2004, **5**, 727-731 (DOI:10.1021/bm034269x).

51 K. K. Chawla, *Fibrous Materials,* Cambridge University Press, Cambridge, U.K., 1998.

52 M. Tian and R. V. Lewis, *Applied Physics A-Materials Science & Processing*, 2006, **82**, 265-273 (DOI:10.1007/s00339-005-3433-8 ER).

53 M. Z. Tian and R. V. Lewis, *Biochemistry,* 2005, **44**, 8006-8012 (DOI:10.1021/bi050366u).

54 T. A. Blackledge, J. Pérez-Rigueiro, G. R. Plaza, B. Perea, A. Navarro, G. V. Guinea and M. Elices, *Sci. Rep.*, 2012, **2**, 782 (DOI:10.1038/srep00782).

55 Y. Takahashi, *Silk Polymers,* 1994, **544**, 168-175.

56 M. Wojcieszak, A. Percot, S. Noinville, G. Gouadec, B. Mauchamp and P. Colomban, *J. Raman Spectrosc.*, 2014, **45**, 895-902 (DOI:10.1002/jrs.4579).